Crystallographic analysis of temperate ice on Rhonegletscher, Swiss Alps

Sebastian Hellmann[1,2], Johanna Kerch[3], Ilka Weikusat[3,4], Andreas Bauder[1], Melchior Grab[1,2], Guillaume Jouvet[5,6], Margit Schwikowski[4], and Hansruedi Maurer[2]

[1]Laboratory of Hydraulics, Hydrology and Glaciology (VAW), ETH Zurich, Zurich, Switzerland
[2]Institute of Geophysics, ETH Zurich, Zurich, Switzerland
[3]Alfred Wegener Institute Helmholtz Centre for Polar and Marine Research, Bremerhaven, Germany
[4]Department of Geosciences, Eberhard Karls University, Tübingen, Germany
[5]University of Zürich, Department of Geography, Switzerland
[6]ETH Zürich, Autonomous Systems Laboratory, Switzerland

Correspondence: Sebastian Hellmann (sebastian.hellmann@erdw.ethz.ch)

Abstract. The crystal orientation fabric (COF) was studied at an ice core that was obtained from the temperate Rhonegletscher, located in the Central Swiss Alps. Seven samples, extracted at depths between 2 and 79 m, were analysed with an automatic fabric analyser. The COF analysis revealed conspicuous four-maxima patterns of the c-axis orientations at all depths. Additional data, such as microstructural images, produced during the ice sample preparation process, were considered to interpret

5 these patterns. Furthermore, repeated high-precision Global Navigation Satellite System (GNSS) surveying allowed the local glacier flow direction to be determined. The relative movements of the individual surveying points indicated horizontal compressive stresses parallel to the glacier flow. Finally, numerical modelling of the ice flow permitted ~~to estimate~~ the local stress distribution. An integrated analysis of all the data sets provided an explanation for the observed four-maximum patterns in the COF. The average azimuths and colatitudes of the c-axes of the individual core samples align with the compressive

10 stress directions obtained from numerical modelling. The clustering of the c-axes in four maxima surrounding the predominant compressive stress direction is most likely the result of a fast migration recrystallisation in combination with the presence of significant shear stresses. This interpretation is supported by air bubble analysis of the LASM images. Our results indicate that COF studies, which were so far predominantly performed at cold ice samples from the polar regions, can also provide valuable insights on the stress and strain distribution within temperate glaciers.

1 Introduction

15

Since the second half of the last century, ice cores have been regarded as extremely valuable archives for reconstructing the climate history of the past hundred-thousands of years (Robin et al., 1977; Petit et al., 1999; Thompson et al., 2002). For example, correlations between ice accumulation, isotopes and dust content have been established, but the deformation of ice layers complicates dating and interpretation of climate records (Jansen et al., 2016). Microstructural analyses have been used

20 to overcome these issues (Faria et al., 2010). In addition ~~to that~~, microstructural investigations ~~are also~~ conducted to reconstruct the ice flow of ice sheets in Greenland and Antarctica as well as in glaciated mountain areas (Russell-Head and Budd, 1979;
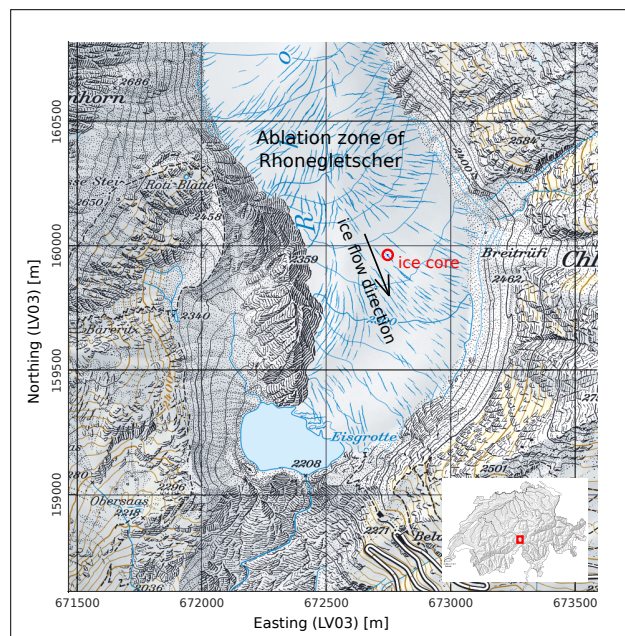
Alley, 1992; Azuma, 1994). For those investigations, the focus has been on the crystallographic orientation of the ice grains. The stresses occurring within the ice mass do not only cause glacier flow, but also induce the development of a characteristic COF and microstructural anisotropy (Faria et al., 2014a).

25   During the past decades, COF and texture have been investigated intensively on polar deep ice cores to understand the microstructure of polycrystalline ice in the context of its deformation history (Hooke, 1973; Gow and Williamson, 1976; Thorsteinsson et al., 1997; Patrick et al., 2003; Gow and Meese, 2007; Montagnat et al., 2014; Weikusat et al., 2017). A historical summary of these projects can be found in Faria et al. (2014a). For the selected ice core drilling spots on domes and ridges, vertical compression and horizontal extension within the ice mass have been found to be the dominant driving stress for ice

30   deformation. In contrast, for ice samples from temperate glaciers, the deformation is dominated by a series of quickly changing simple and pure shear conditions along the valley in combination with basal sliding, which results in a much more complex history (Hambrey and Milnes, 1977). This requires more extensive analyses of COF. First crystallographic investigations have been performed on temperate glaciers already in the 1950's to 1980's, including the detailed investigations of Kamb (1959) and Rigsby (1960), and later extended by Budd (1972), Hambrey and Milnes (1977), Hooke and Hudleston (1978), and Hambrey

35   et al. (1980). A potential problem of temperate glacier crystal analysis is the large grain size and thus limited amount of grains that can be analysed for each sample. This may be the reason, why a surprisingly low number of papers was published on crystal structure of temperate glaciers (e.g. Tison and Hubbard, 2000) during the past years. Furthermore, the majority of the earlier studies mainly analysed samples from the uppermost few meters.

The ice of temperate glaciers is comparable with a metamorphic rock close to its melting point (Hambrey and Milnes, 1977)

40   that has been exposed to a long series of deformation processes along the valley. This deformation is caused by various shear and compressional stresses that have been applied to the ice. These stress regimes produce heterogeneously distributed dislocations, which cause dynamic recrystallisation by rearrangement of these dislocations or by internal strain energy reduction. The resulting recrystallisation processes and the interplay between deformation and recrystallisation in the ice take place even faster as the temperature gets closer to the pressure melting point (Alley, 1988; Weikusat et al., 2009a). As a result, the adaption

45   of the ice crystal structure to new stress conditions is expected to be faster (e.g. Kamb, 1972; Duval, 1979). Additionally, the higher temperatures provide more thermal energy and allow a faster grain growth (Azuma et al., 2012), leading to an interplay between stress and temperature regime (Alley, 1988; Faria et al., 2014b). Therefore, large differences can be observed between cold and temperate ice. One of the most apparent differences is the grain size, which has been found to be a few centimetres in temperate ice (Rigsby, 1960), whereas samples from polar ice usually show grains with a diameter of a few millimetres, except

50   in deepest parts, where temperatures rise close to the pressure melting point (e.g. Gow and Williamson, 1976; Thwaites et al., 1984; Kuiper et al., 2019).

Although ice core drilling and preparation of thin sections is still a time-consuming process, and only a few discrete measurements are possible within a reasonable amount of time, the technique for analysing COF has developed extensively, for example, by using image analysis software and powerful computing resources (Wilson et al., 2003; Peternell et al., 2009; Wil-

55   son and Peternell, 2011; Eichler, 2013).

In this study, we analyse ice core samples from a temperate alpine glacier. We describe and compare our findings with studies
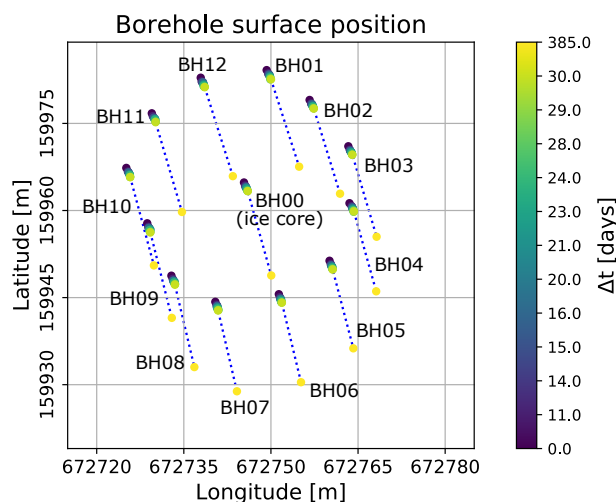
Figure 1. Rhonegletscher ablation area, ice core position indicated in red, ice flow direction at ice core location shown by black arrow.

from the last century and provide a hypothesis for the resulting COF in terms of given stress and temperature conditions. We analyse the stress regime in the vicinity of the ice core, using additional borehole measurements and discuss recrystallisation processes and grain growth in temperate ice. For selected examples we take a closer look at the development of new ice crys-

60   tals under the current stress regime of the glacier. The microstructural results of this study serve as a basis for geophysical experiments on ice core samples, which will be discussed in an accompanying paper, and they can be compared with results from larger scale geophysical experiments.

2   Field Site and Data Acquisition

The field work was carried out on Rhonegletscher, located in the Central Swiss Alps (Fig. 1). This glacier currently covers

65   an area of about $15.5\,\mathrm{km^2}$ and is flowing in southern direction from $3600\,\mathrm{m}$ a.s.l. down to $2200\,\mathrm{m}$ a.s.l. It is a medium-sized valley glacier, easily accessible, and therefore investigations were carried out already in the last two centuries and continuously since 2006 (Bauder, 2018).

In August 2017, the ice core was drilled in the ablation area of the glacier (Fig. 1), approximately $500\,\mathrm{m}$ north of its current terminus. Here, the ice was flowing with an average surface velocity of $16.2\,\mathrm{m\,a^{-1}}$ in the season 2017/18 according to GNSS

70   measurements. This location was selected, because the glacier surface forms a relatively even plateau with only $5\,\mathrm{m}$ elevation change over a distance of $40\,\mathrm{m}$ and is free of crevasses. Further up-glacier there is a steep and crevassed area. An analysis of the bedrock with ground-penetrating radar measurements also confirmed a transition from a steep to a more flat zone of the

3

The Cryosphere

Discussions

Open Access

EGU

Figure 2. Analysis of ice flow direction, the displacement of the borehole surface points measured by GNSS is shown for each borehole with colours indicating the time since drilling.

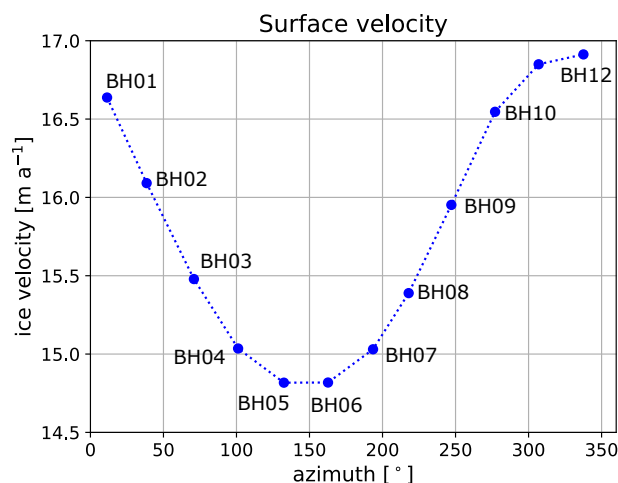valley (Church et al., 2018) at the ice core location.

As the ice is just at the pressure melting point, a thermal drilling technique (Schwikowski et al., 2014) was used. Although
75 hot-water drillings, performed in the vicinity of the ice core location, showed a mean ice thickness of 110 m, the drilling was
stopped at 80 m, when hitting some gravel, which blocked the cutter head. An 80 m long ice core, with a gap between 46 and
50 m due to technical issues, was retrieved.

Due to the thermal drilling technique, which did not apply a rotational force onto the ice core segments, an oriented retrieval
of the segments was possible. A freshly drilled segment was manually connected to the previous one, which worked out well
80 for most of the segments. Additional measurements of the Earth's magnetic field, while drilling, could be used in some cases
to reconstruct the orientation within a range of $\pm 10°$ when matching of neighbouring segments was not possible.

To complement the results of the ice core analysis, we made use of an array of hot-water-drilled boreholes surrounding the loca-
tion of the ice core retrieval (Fig. 2). The locations of the borehole collars were surveyed repeatedly using high-precision GNSS
measurements. The displacements of the borehole collars indicate a south-eastern flow direction with an azimuth of about 155°
85 $\pm 10°$. Besides determining the general flow direction from the absolute movements of the borehole collars, their relative
displacements provided further insights. In Fig. 3, the displacements of the individual boreholes are plotted. The south-eastern
boreholes (BH04 to BH07) show significantly smaller displacements, compared with the boreholes located in the north-western
part of the array (BH01 and BH10 to BH12). This indicates compression of the ice in this region.

To support these observations at the surface, the conditions inside the glacier were investigated with a numerical ice flow
90 model. We modelled the dynamics of the whole Rhonegletscher using the Elmer/Ice model (Gagliardini et al., 2013), which
solves the full Stokes equations based on Glen's flow law. Here we simply ran the stationary model without any time evo-
lution. Main model inputs are a bedrock model and surface topographic information, as well as sliding coefficient and rate

4

Figure 3. The ice flow analysis shows the absolute horizontal displacement of the borehole collars from GNSS after 385 days for each borehole around the ice core hole (borehole azimuthal direction relative to ice core hole, N=0°).

factor that control the amount of basal motion and internal deformation, respectively. The bedrock model was obtained from GPR measurements (Church et al., 2018) and from a Swiss-wide glacier inventory that is currently being updated (GlaThiDa Consortium, 2019; Farinotti et al., 2009; Grab et al., 2018). As rate factor, we choose $A = 100\,\mathrm{MPa}^{-3}\mathrm{a}^{-1}$, which was tuned for modelling Aletschgletscher (Jouvet et al., 2011) and a homogeneous sliding coefficient $c = 10\,\mathrm{km\,MPa}^{-1}$. We tuned the sliding coefficient such that the observed and modelled ice velocities match at the surface of the borehole. As outputs from the Elmer/Ice model, we obtained the velocities and stress field.

3 Crystal Orientation Fabric Analysis

For detailed structural investigations of the temperate glacier ice, a COF analysis was performed in the laboratories of the Alfred-Wegener-Institute Helmholtz Centre for Polar and Marine Research (AWI). The orientation of the c-axes of the ice grains were ~~analysed to determine the orientation of the crystals~~. The c-axis is the symmetry axis perpendicular to the basal plane of a hexagonal crystal. Along the c-axis, the physical properties, such as bulk and shear modulus, differ significantly from any direction parallel to the basal plane (the a-axes). The elastic parameters of the ice, such as bulk or shear modulus, have enhanced values and the crystal is more resistant ~~against~~ deformation (Cuffey and Paterson, 2010, chapter 3). This results in anisotropy effects, which lead, for instance, to different velocities for acoustic waves travelling through the ice (e.g. Diez and Eisen, 2015).

From the ice core extracted from the central borehole BH00 (Fig. 2), seven samples at depths of 2, 22, 33, 45, 52, 65 and 79 m were considered. Due to technical problems during the core retrieval, the azimuthal orientations of the samples at 2 and 45 m depth are subject to some uncertainties. Their azimuthal orientations were thus obtained from extrapolations from adjacent

measurements.

Each of the seven samples consisted of an ice core segment of about 50 cm length. Up to four 11 cm long adjacent sub-samples (Fig. 4) were prepared from each of these segments. Each sub-sample was then further dissected into a horizontal and two vertical cuts, all three perpendicular to each other (Fig 4). This resulted in a horizontal circular slice and two vertical slices

115 with SN- and EW-orientations from which thin sections were prepared. Between 8 and 12 thin sections per sample and 77 thin sections in total were measured. This procedure enabled a more comprehensive analysis of the large crystals existing in temperate glacier ice (e.g. Kamb, 1959; Rigsby, 1960) and fractures, for instance from potential meltwater intrusions. The dimensions of the pieces were 10×6 cm for the vertical sections and a diameter of ≈ 7 cm for the circular horizontal sections. The creation of sub-samples and choosing three different types of sections (horizontal, EW-vertical, SN-vertical) for every

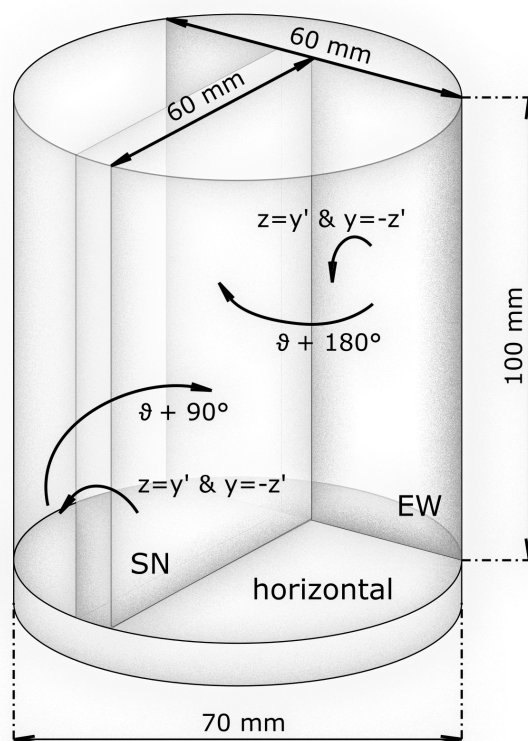120 sub-sample resulted in a comprehensive analysis of at least 300 grains for each depth level.

During the preparation of the ice thin sections, large-area scanning macroscope (LASM) images (Binder et al., 2013; Krischke et al., 2015) were taken from the polished surface of the 1 cm thick ice samples. As discussed later, these images provide important information on the grain boundary network as well as the air bubble distribution, since light from the active camera is backscattered to a great extend by the evenly polished ice surfaces. Uneven parts, such as air bubbles or grain boundaries,

125 reduce the amount of backscattered light and appear darker in the image.

All sections were analysed using polarised light (Wilson et al., 2003; Peternell et al., 2009). The automatic fabric analyser G50 from Russell-Head Instruments (Wilson et al., 2003) was used to measure the orientation of the c-axis on a predefined mesh grid with a pixel resolution of $20 \times 20\,\mu m^2$. The c-axis of an ice crystal is determined by two angles:

$$\boldsymbol{c}(\vartheta, \varphi) = [\cos(\vartheta)\sin(\varphi),\ \sin(\vartheta)\sin(\varphi),\ \cos(\varphi)]. \tag{1}$$

130 The first angle defines the azimuth $\vartheta \in [0, 2\pi]$ of the c-axis in the horizontal plane. The second angle is the colatitude $\varphi \in [0, \frac{\pi}{2}]$ from vertical.

For the postprocessing of the obtained crystallographic data, the software *cAxes* (Eichler, 2013) was used. *cAxes* analyses the misorientation angle between the determined c-axis orientations of neighbouring pixels and combines those with a misorientation $< 1°$ to individual ice grains with a mean c-axis azimuth and colatitude per grain. The minimum grain size, calculated

135 from the number of pixels multiplied by the pixel resolution, was set to $0.2\,\mu m^2$ (500 pixels). Vertical thin sections (Fig. 6, SN/EW) were rotated around the horizontal x-axis x' of the local measurement coordinate system (x', y', z') by $90°$ into the ice core system (z = core's vertical axis) ($z = y'$ and $y = -z'$). Then, they were rotated towards the reference point that was engraved into the core segments (e.g. $\theta_{EW} = \theta_{EW} + 180°$). In a final step, the magnetometer data were used to obtain the true azimuthal orientation for all thin sections of a sampling depth relative to geographic north. This ensures an identical coor-

140 dinate reference frame for all types of thin sections along the whole ice core. Finally, the eigenvalue distribution according to the procedure of Wallbrecher (1986) was computed. The three eigenvalues a_i (i=1, 2, 3) follow the relations $\sum a_i = 1$ and $0 \le a_3 \le a_2 \le a_1 \le 1$. These eigenvalues represent the main axes of an ellipsoid which presents the best fit for a given c-axis density distribution.
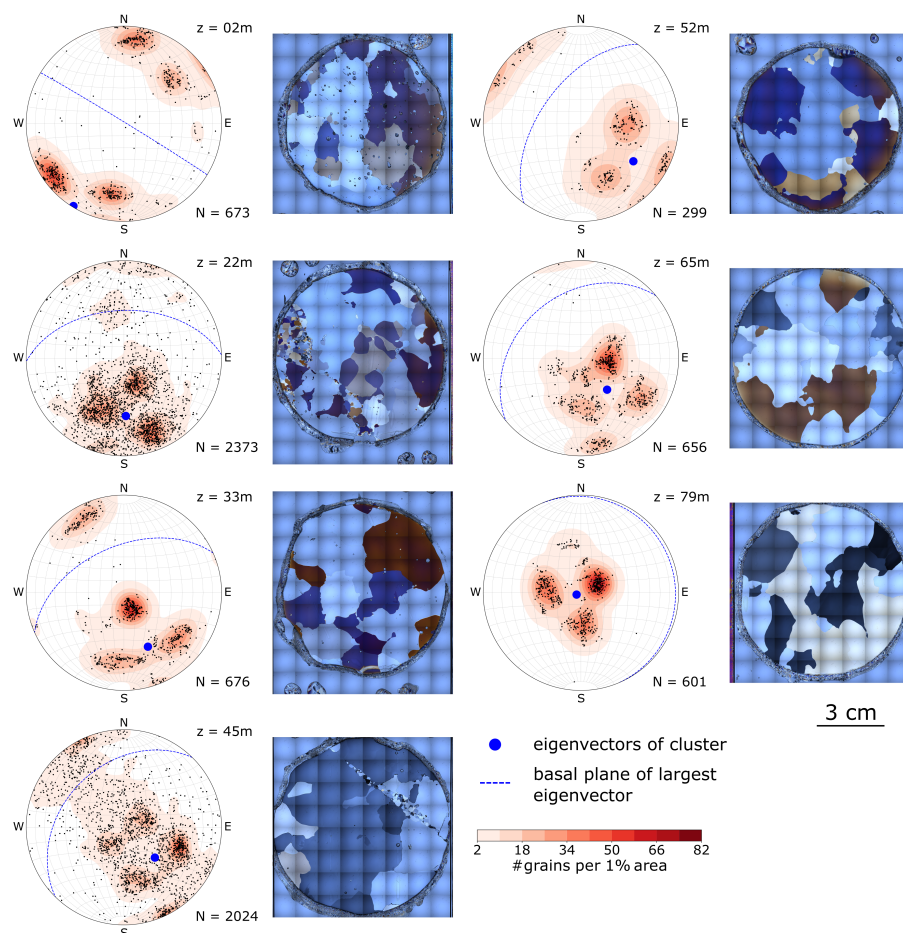
The Cryosphere
Discussions
Open Access
EGU

Figure 4. Cutting scheme for the ice core analysis. An 11 cm long piece of the ice core was cut in a horizontal (d=7 cm) and two vertical (east-west, south-north oriented, 10x6 cm) thin sections. Four thin sections of each type were analysed and combined per sampling depth.

4 Results

145   Figure 5 shows the results of the COF analysis (left panels) and selected images of horizontal cross-polarised thin-sections (right panels) for each depth level. The COF results are displayed in form of Schmidt equal-area ~~stereo~~ plots on the lower hemisphere (vertical core axis in centre). Results from all sub-samples and section orientations are combined. Each ice grain c-axis is represented by a dot. As shown by the images of cross-polarised thin sections in the right panels of Fig. 5, the ice matrix is dominated by a few extremely large grains. Nevertheless, several hundred small grains appear along the grain boundaries

150   or in specific patches. Especially the samples from 22 m and 45 m contain a large number of small grains. These grains form specific patterns looking like fractures or fissures, which are traceable through several thin sections.

For better visualising the c-axis distributions, a smoothed colour density plot, calculated in accordance to Kamb's method (Vollmer, 1995), was superimposed on the stereo plots. These density plots only consider the number of grains within the area of the stereo plot, i.e. the size of the individual grains does not affect the colour code. All density plots indicate a multi-maxima

155   pattern, ~~whereby~~ the majority exhibits four maxima. The orientation of the patterns varies with depth, but the structure inside

Figure 5. Stereo plots (lower hemisphere Schmidt equal-area projection into the horizontal, i.e. long axis of core is in the centre) with the final c-axis distribution and horizontal thin sections, illustrating the typical grain size distribution, are shown for each sample. The total number of ice grains (N) is specified for each sample (consisting of at least 3 horizontal and 6 vertical thin sections, all rotated to horizontal view and common geographic coordinates). The sampling depth (z) is indicated in the upper right corner of the stereo plots. The colour code (smoothed Kamb's distribution (Vollmer, 1995)) emphasises the existing clusters of the c-axis distribution. The largest eigenvector for the determined distribution is depicted as blue dot and its normal plane is shown as dashed line.

the pattern is remarkably similar. The four maxima lie on a small circle girdle, which is characterised by an opening angle around a central vector, shown as a centroid in the stereographic projection. Two maxima always lie on opposite sides of this centroid and the other two on a line perpendicular to the first two clusters so that the azimuthal distribution of the maxima is 90°. Deviations are observed at 45 m depth, where a fifth maximum at the horizontal margin appears, and at 79 m, where one

160   of the four maxima is significantly weaker.

The eigenvectors of the polycrystalline orientation tensor were calculated for each depth, and they are also shown in the stereo plots (blue dots in Fig. 5). For an enhanced visibility, the normal plane for the eigenvector associated with the largest eigenvalue is indicated with a dashed blue line. This eigenvector is plotting in the centre of the four-point-maximum. The opening angle between the largest eigenvector and the individual maxima varies with $\pm 15°$ around a mean of 30° (Table 1), but the mean

165   value is constant over all depths.

With an exception for the uppermost depth at 2 m, the COF patterns in the upper part of the ice core are oriented in the direction of the glacier's ice flow (c.f. Figs. 1, 2). With increasing depth, the centre of the c-axis distribution has a decreasing colatitude, and at 79 m the largest eigenvector is almost vertically oriented.
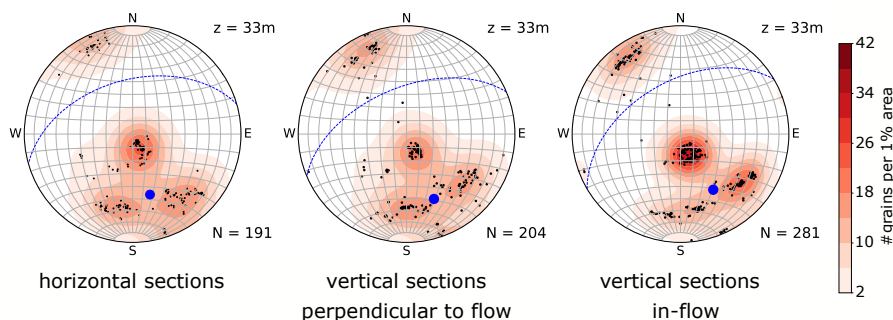
Table 1. Angles between individual maxima and the centroid, i.e. the largest eigenvector, describing the relative geometry of the multi-maximum pattern and the absolute position (azimuth/colatutide) of the centroid

depth [m]	relative angles within the cluster					absolute position of cluster	
	angles per maximum [°]				mean angle [°]	azimuth [°]	colatitude [°]
2	23.3	27.4	34.3	34.5	29.9 ± 4.7	211.5 (151.5)	88.6
22	23.5	25.3	34.5	35.2	29.6 ± 5.2	178	49.4
33	20.8	26.0	41.0	47.6	33.9 ± 10.9	156	50.6
45	26.9	29.2	30.7	33.2	30.0 ± 2.3	134.4	36.6
52	22.2	27.9	29.6	38.2	30.6 ± 5.7	125.6	55.7
65	20.6	22.5	34.7	37.6	28.9 ± 7.4	140.2	34.5
79	20.2	25.2	34.3	34.6	28.6 ± 6.1	246.6	3.9

For an enhanced and statistically significant data set, we combined the determined c-axis orientations, measured in up to twelve

170   individual thin sections with three different orientations. However, the results from the different orientations of the sections (Fig. 4) may be inconsistent. Although the grains are not elongated in a certain direction, some of them appear branched and interlocked (Fig. 5, right panels). Therefore, two-dimensional cuts through large, branched grains may let them appear as several individual grains within the same section. This could result in over-represented clusters in individual thin sections, which appear in the superimposed stereo plots from the different sub-samples.

175   To check the consistency of the individual orientations, the c-axis distribution for each sub-section (horizontal, east-west and south-north) was analysed separately. Figure 6 shows the results for the sample at 33 m depth. All three sub-sections show a similar pattern. The individual maxima appear in all sections and are not a result of stitching differently orientated sections

Figure 6. Stereo plots (lower hemisphere Schmidt equal-area projection) for the three types of sub-samples (horizontal, east-west, south-north, from left to right). Number of grains N is given for each type of sub-sample. The colour code (smoothed Kamb's distribution (Vollmer, 1995)) emphasises the maxima of the c-axis distribution. The blue dot indicate the largest eigenvector and the dashed blue line indicate its normal plane.

together. However, due to the afore-mentioned reasons, the actual grain size is difficult to determine. Individual analyses for the other depths showed similarly consistent results (not shown).

5   Interpretation

The results, shown in Fig. 5, exhibit fairly consistent patterns that can be explained in terms of glacier dynamics. Here, we provide an interpretation of three significant features, namely

- the azimuthal orientation of the c-axes,

- the decrease of the ~~c-axis~~ colatitudes with increasing depths, and

- the existence of multi-maxima patterns in the c-axis distributions.

To aid the interpretation, the stereo plots in Fig. 5 are shown again in Fig. 7 with adjustments as a result of the following interpretation. Here, only the colour-coded c-axis distributions are plotted, superimposed by additional information obtained from accompanying analyses.

5.1   Azimuthal orientation

Results from all depth levels, with the exception for 2 m, show in general a mean c-axis orientation (Table 1) parallel to the main glacier flow direction that was obtained from the displacements of the surrounding boreholes (Fig. 2, ≈155°). As a result of the horizontal compression (σ_{xx}), determined from the relative movements of the surrounding boreholes (Fig. 3), the azimuths of the c-axes are aligned with the azimuth of this compressional stress. This is in accordance with results from laboratory experiments in a number of previous studies (e.g Kamb, 1972; Duval, 1981; Budd and Jacka, 1989) and comparable with some

195   parts of the Cape Folger ice core (Thwaites et al., 1984).

The uppermost sample (2 m) does not fit into this interpretation. Although the magnetometer data are consistent, the onset between two segments at 10 m was unclear and we cannot fully exclude a misorientation between the segments in 2 and 22 m. As shown in Fig. 7 an azimuthal correction of -60° would lead to a perfect alignment of this sample with all other observation and the modelling results for the particular location. Therefore, we assume a misorientation of the core segments. However,

200   the orientation of the pattern in 2 m is in alignment with the glacier flow about 800-1000 m up-glacier (Fig. 1). As the absolute stress and strain rates are lower at the surface, the pattern close to the surface might not be reshaped in the last 1000 m of ice flow and thus show the remnant orientation further up-glacier when the ice was buried deeper in the glacier and thus exposed to higher absolute stress and strain rates.

5.2   Colatitude variations

205   Here, we consider the variations of the colatitude of the largest eigenvector (Fig. 7). There is a decrease of the colatitude from 89° to 4° with increasing depth (Table 1). This is likely the result of the stress and strain distribution in the glacier. Generally, the c-axes of the ice crystals orient themselves parallel to the ice flow, which coincides with the modelled maximum compressive stress (σ_1) direction. As indicated by the relative movements of the surrounding boreholes (Fig. 3), we observe a compression parallel to the glacier flow at the glacier surface. Based on borehole inclination measurements (not shown), it can

210   be further assumed that the flow-parallel compression also occurs at greater depths. However, with increasing depths, the ice overburden generates an additional vertical stress component. This causes an increasing vertical deformation of the ice which lets the c-axes rotate towards a vertical direction with increasing depths, and explains, at least qualitatively, the observations in Fig. 7.

The principle compressive stress orientations (σ_1), modeled with the Elmer/Ice model, were added to Fig. 7 (green dots in the

215   stereo plots) for comparison. Although not matching perfectly, a generally good agreement between modelled and observed largest eigenvector directions (blue dots) is observed in Fig. 7, thereby supporting our interpretation. However, the discrepancy might be a hint that the c-axis distribution is governed by strain (and not stress) in the last consequence (Budd et al., 2013; Faria et al., 2014b). Especially in the presence of simple shear, the direction of stress and strain are not necessarily aligned anymore, in particular for recently formed ice grains (non-coaxial relation) (Duval, 1981).

5.3   Multi-maxima c-axes distribution

If the c-axis orientations would be governed solely by the orientation of the principal compressive stress direction (σ_1), we should observe a single maximum in the stereo plots. However, as observed in Figures 5 and 7, this is not the case. Instead, the orientations deviate on average about 30° from the principle stress direction (indicated by black circles in Fig. 7).

A possible explanation of this observation includes recrystallisation processes. As described in Duval and Castelnau (1995) and

225   Schulson and Duval (2009, chapter 6), it can be distinguished between rotation recrystallisation, which is observed primarily in cold ice (e.g. Lipenkov et al., 1989), and migration recrystallisation, which seems to be the dominant mechanism in temperate ice near the pressure melting point (e.g. Gow and Williamson, 1976; Azuma and Higashi, 1984). In a more recent work of Faria

et al. (2014b), these processes are no longer just attributed to temperature, but to temperature in combination with ~~cumulative~~ strain and the term dynamic recrystallisation is used. In any case, dynamic grain growth and the formation of new nuclei

230 are dependent on temperature, as the grain boundary mobility depends on the general energy state of the system, and strain rate due to dislocations being formed during deformation. Under constant strain rates, higher temperatures cause an increased grain growth (Schulson and Duval, 2009, chapter 6) and a faster recrystallisation in case of ~~inadequately~~ oriented grains and heterogeneous distribution of dislocations in neighbouring grains (Weikusat et al., 2009b, Fig. 8).

As explained in Cuffey and Paterson (2010, chapter 3), c-axis orientations, resulting from migration recrystallisation tend to

235 deviate from the principle compressive stress direction (σ_1), as observed in Fig. 7. If the recrystallisation would be the result of an unconfined compression only, one should observe a continuous distribution of the c-axes along the small circle girdle (black circles in Fig. 7). Instead, the orientations typically cluster around four maxima lying on these circles. As shown in Figure 3.7 in Cuffey and Paterson (2010, chapter 3), this can be explained by a combination of compressional and shear stresses. The modelled stress tensor provides hints for increasing shear stresses (τ_{xz}) with depth, and also borehole inclination

240 measurements provide some evidence for the occurrence of shear stresses. The borehole trajectories of all 12 boreholes around the core location show typical parabola-shaped curvature 50 m below the surface four weeks after drilling.

Our interpretation is based on the assumptions that (i) strain-induced boundary migration (SIBM) occurs in the investigation area, and (ii) that all crystals have been recrystallised recently. The former requires temperatures near the pressure melting point. Concerning the later and following the most recent research of Faria et al. (2014b), a change in the strain rate due to

245 different flow direction in the glacier would lead to a grain size reduction regime. The existing grains start to recrystallise, and the newly oriented grains grow until they reach again the steady state, which depends on temperature, grain~~s~~ size and strain rate (which is directly related to stresses in magnitude). As this is a continuously ongoing process, we can expect a direct relationship between current stress and thus strain rate and the orientation under constant temperature conditions. This interpretation is also in good agreement with findings in Budd and Jacka (1989).

250 Evidence that the crystals must have formed near the pressure melting point, can be found in the images of cross-polarised thin section (right panels in Fig. 5) and in the grain size distribution provided in Table 2. Evidently, our samples include very large crystals, and there is a considerable variability of the grain sizes at all depths. This is indicative for crystal formation near the pressure melting point (Gow and Williamson, 1976; Jacka and Jun, 1994), which in turn allow an extremely fast grain growth (Alley, 1992). These observations are further supported by derived temperature profiles in a 25 m deep tunnel close to

255 the glacier snout clearly indicating temperate conditions of > -1°C (personal comm. M. Lüthi, 2019).

Supporting arguments for a fast and complete dynamic recrystallisation of the individual grains are provided by the distribution of air bubbles, found in the LASM images. An example of a LASM scan, obtained from 2 m depth, is shown in Fig. 8. It exhibits bubble-free (top part) and bubble-rich (bottom part) areas. Similar distributions were found at other depth levels, although the amount of air bubbles generally decreases with increasing depths.

260 In polar ice, air bubbles are usually found along grain boundaries. They often migrate, when ice grains are growing (Alley et al., 1986), as they can be regarded as an energetic obstacle in the crystal lattice. In the LASM scans in Fig. 8, such air bubbles are observed as well (encircled with dashed red lines). However, there are also bubbles completely trapped within the ice grain

matrix (encircled with dashed green line) and some air bubbles, which are still part of the grain boundaries, but causing a bending of these boundaries and the development of new sub-grain boundaries on the opposite side of the air bubble (encircled

265 with dashed blue line). The ~~later~~ two air bubble types are evidence for an extremely fast boundary migration process and fast growing ice crystals.
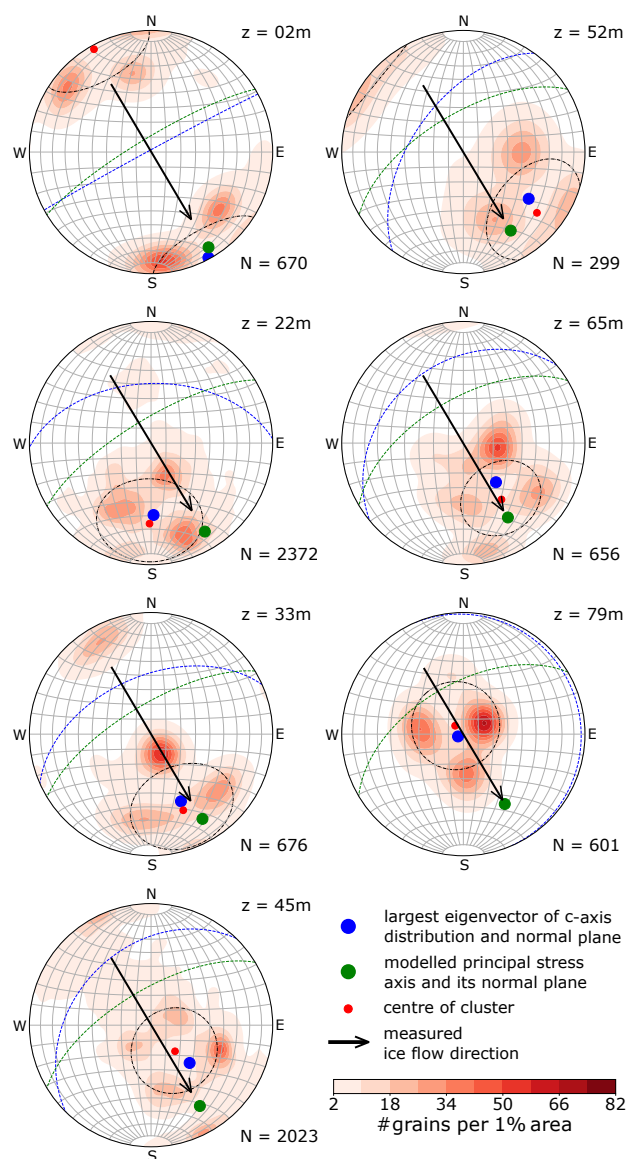
Table 2. Grain size distribution (mean and maximum grain sizes [mm^2], minimum grain size is $0.2\,mm^2$ and defined as threshold during processing)

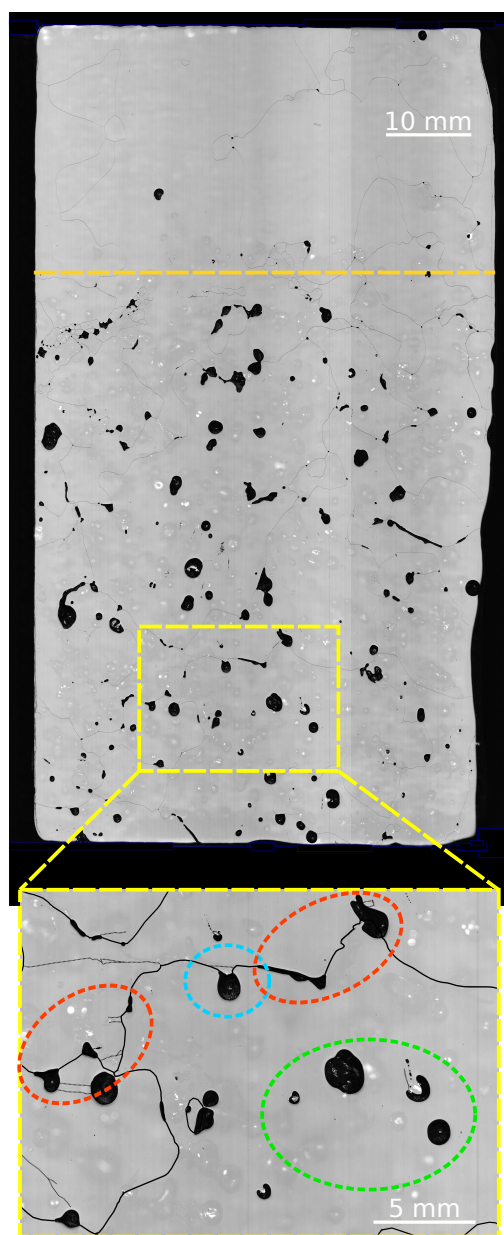| depth [m]	number of grains	mean	max
2	673	77.06	1826.71
22	2373	19.04	1551.97
33	676	85.97	3994.17
45	2024	29.89	3249.29
52	299	121.42	1986.70
65	656	95.02	3752.65
79	601	96.79	3236.18

6 Discussion

The literature on COF field studies is not conclusive concerning the existence of multi-maximum fabrics. They were observed in early studies on temperate glaciers (e.g., Rigsby, 1951; Kamb, 1959; Rigsby, 1960; Hooke and Hudleston, 1980), and also

270 in the bottom ice of Byrd Station and Cape Folger in Antarctica (Gow and Williamson, 1976; Thwaites et al., 1984) and often referred as "diamond-shape" pattern or fabrics. At that time, the estimation of c-axis distributions was more subjective and could not benefit from modern equipment, as employed in our study. The orientation of crystals was determined manually on a Rigsby-stage by turning and tilting the ice samples between polarised plates. Thus, only a limited number of grains (up to 100) and usually the largest grains were analysed. Therefore, the "diamond-shape" pattern was debated to be a statistical or

275 method-immanent effect.

Interestingly, in more recent studies on other temperate glaciers multi-maximum fabrics in combination with a large grain size were only observed in the deepest parts of the ice cores (e.g. Tison and Hubbard, 2000). However, following the argument~~ation~~ in Faria et al. (2014b), strain-induced boundary migration (SIBM) and grain growth is not a result of temperature alone. Grain growth and the formation of new grains depends on temperature and strain rate. Most likely, the observed "diamond shape"

280 pattern only develops under strain-induced boundary migration from new grains (SIBM-N) at high strain rates, in contrast to SIBM-O which already takes place at lower strain rates (under similar high temperature conditions) and in which the old grains are still in place (Faria et al., 2014b, Fig.13+14). The conditions for a "diamond-shape" pattern seem to be suitable in larger glaciers like the Rhonegletscher, whereas in smaller and thinner glaciers, such as Glacier de Tsanfleuron investigated in Tison

Figure 7. Stereo plots (lower hemisphere Schmidt equal-area projection) with the colour coded (same as Fig. 5) final c-axis distribution for each sample are shown. The total number of ice grains is specified for each sample. The black dashed line shows the mean opening angle for the cone of maxima around the centroid depicted as red dot. The calculated largest eigenvector for the c-axis distribution is shown as blue dot (its normal plane as dashed blue line) and the calculated largest principal stress axis from the ice flow model is represented by a green dot (its normal plane as dashed green line).

Figure 8. Example of a LASM image indicating several processes in the temperate ice: black areas are air bubbles and black lines represent the grain boundaries. Black dashed lines indicate subgrain boundaries. Air bubble rich ice and air bubble free ice have relatively sharp boundaries as indicated by the dashed orange line. Air bubbles are part of grain boundaries (red circles in zoomed image) but also completely trapped within individual large ice grains (green circle in zoomed image). An intermediate state of incorporating air bubbles is shown in the blue circle.
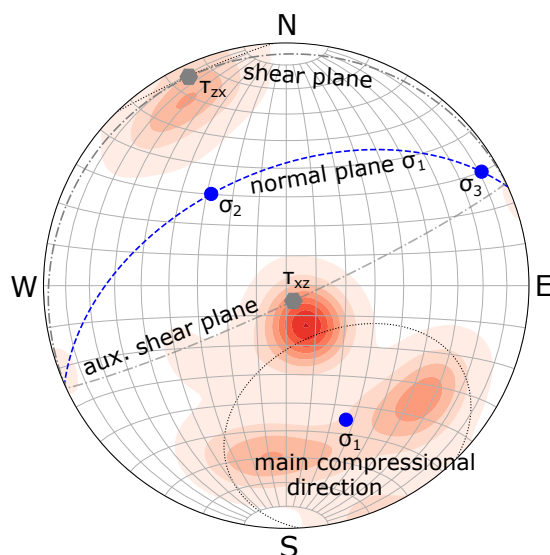
and Hubbard (2000), the strain rates might be smaller due to the lower ice thickness and thus the multi-maxima patterns develop

285   only in the deepest parts with presumably the highest strain rates. In contrast, in polar ice cores the strain rates are expected to be large enough, but only in the deepest parts also the temperature conditions are fulfilled for multi-maximum fabrics as observed in some Antarctic and Greenlandic cores (Gow and Williamson, 1976; Thwaites et al., 1984; Montagnat et al., 2014). The results of Thwaites et al. (1984) for the multi-maximum ice at the base of Cape Folger ice core show the largest similarities (orientation in relation to observed stresses, grain size structure, and the opening angle of the multi-maximum structure) with

290   our results. To sum up this argumentation, multi-maxima patterns only form under high temperatures and high strain rates (SIBM-N case). Only if a certain strain rate is applied to the ice, the pattern is created in alignment with the deformation. This may explain why the COF at the depth of 2 m (Figure 5) does not align with the current glacier flow. The absolute strain rate close to the surface is expected to be lower than deeper in the ice. Presumably, this strain rate at the current location is too low for a SIBM-N to take place and thus the previous orientation when the ice was buried deeper in the glacier and exposed to

295   higher strain rates is preserved. The orientation fits to the flow about 800 m up-glacier.

In contrast, COF laboratory experiments provide clear evidence for multi-maximum fabrics. Kamb (1972); Duval (1981) and Maohuan et al. (1985) performed laboratory experiments on artificial ice under high temperatures (> -2°C), slightly below the pressure melting point. They combined shear and compressional stresses in their torsion-compression-experiments. This is similar to what we expect on Rhonegletscher. In another study, Duval (1981) argued that the multi-maximum centroid is paral-

300   lel with the compressional axis, but he added that two further maxima exist that are parallel to the poles of the two main shear stress plains (vertical and horizontal). Maohuan et al. (1985) applied only a compressional stress onto the sample and showed a development of the structures from a small girdle around the compressional axis at early stages that developed towards a multi-maximum fabric. In addition to that, the opening angles we observe fit quite well to the results of Jacka and Maccagnan (1984) who analysed the opening angle of small circle girdles formed under compressional stress. For such opening angles

305   between compressional direction and the c-axis direction, the compressive strength applied onto the ice crystal is minimised (Schulson and Duval, 2009, chapter 11).

The stresses applied on the samples in these laboratory experiments are in a similar range (σ = 0.24-0.6 MPa (Duval, 1981)) as what we expect from our glacier model for the intermediate and deeper parts (up to 0.7 MPa). As the crystal orientation in these experiments adopted rather quickly towards new stresses under similar temperature and stress conditions, we can expect

310   to have a similar fast adaption in the glacier. Thus, our findings are in good agreement with these laboratory experiments.

Following Cuffey and Paterson (2010), we argue that the existence of multi-maxima fabrics is the result of combined compressional (σ_{xx}) and shear stresses (τ_{xz}). This hypothesis is also supported by microdynamical models (Llorens et al., 2016) and laboratory investigations (Journaux et al., 2019). These investigations provide evidence that simple shear processes in temperate ice produce two maxima, one perpendicular to the shear plane (parallel to the normal vector of that plane) and a second

315   maximum in the direction of shearing. The exact angle between these two maxima depends on the experimental conditions (Qi et al., 2019). Such a horizontal shear plane and its normal vector (τ_{xy}) as well as the auxilliary plane and its normal vector in ice flow direction (τ_{zx}) are shown in Fig. 9. In this specific example, two of the four maxima clearly correlate with such a simple shearing. For the other samples the attribution of particular maxima to simple shearing is not that obvious. The maximum at

Figure 9. Stereo plots (lower hemisphere Schmidt equal-area projection) with principal axes of the c-axis eigenvectors (shown as blue dots), the normal plane for the largest eigenvector (repr. by the blue dashed line) and the plane of simple shear stress and the auxillary plane (perpendicular to the plane of simple shear) with their respective normal vectors (shown as dashed lines and dots in grey colours).

the horizontal margin (τ_{zx}) would vanish over time as the ~~crystals~~ tend to rotate towards the maximum perpendicular to the
320 actual shear plane (Duval, 1981; Llorens et al., 2016; Journaux et al., 2019) and emphasise the vertical maximum (τ_{xz}). The fact that both maxima (τ_{xz} and τ_{zx}) are still visible, fits again to the assumption of a continuous recrystallisation process and relatively young but fast growing ice grains. The grain growth and especially the coarse-grained ice that can be observed in all samples in any depth are clearly a result of the high temperatures and has been observed in ice cores in Antarctica (Byrd (Gow and Williamson, 1976), Cape Folger (Thwaites et al., 1984)) as well as Greenland (GRIP (Thorsteinsson et al., 1997),
325 NEEM (Montagnat et al., 2014)) and in several temperate glaciers (Kamb, 1959; Rigsby, 1960; Hooke and Hudleston, 1980). The largest difference though is most likely the different time horizon for the grain growth, especially compared to the polar cores.

However, there exist alternative explanations. Matsuda and Wakahama (1978) suggest twinning effects that may occur when c-axes develop under recrystallisation. Potentially, these effects may lead to a clustering of the c-axes. This theory is supported
330 by the fact that the opening angles of two opposing clusters are generally similar, whereas the angles compared to the other two maxima can vary within 15-20° and therefore called "diamond-shape" fabrics. Apart from that, it is hard to find any studies about observations on twinning as result of ice deformation in glaciers and Faria et al. (2014b) summarised that mechanical twinning has not been observed in glacier ice ~~yet~~.

335 **7 Conclusions**

COF analyses of an ice core, extracted from a temperate alpine glacier, showed conspicuous multi-maximum patterns of the c-axes. This was observed at different depth levels. Generally, the azimuths of the c-axes point in the direction of the glacier flow, which coincides at the test site with the maximum compressive horizontal stress direction. At the surface, the c-axes are thus predominantly horizontal, but with increasing depths, their colatitudes decrease. Ice flow modelling results support the

340 assumption that this is an effect of combined compressive horizontal stresses in ice flow direction and depths-increasing vertical stresses caused by the ice overburden. The presence of multi-maxima patterns (instead of a single maximum) can be explained by (i) migration recrystallisation and (ii) the presence of shear stresses. The multi-maximum patterns are also indicative that a fast and complete migration recrystallisation must have occurred. This interpretation is supported by air bubble analyses in LASM images.

345 To the best of our knowledge, this is the first comprehensive COF analysis of an ice core from a temperate alpine glacier that links the COF with the glacier flow. The results are consistent with supporting measurements and modelling results. These consistencies are encouraging, and will hopefully motivate similar studies on other temperate glaciers.

Data availability. The ice fabric data are published in the open-access database PANGAEA® (Hellmann et al., 2018) and are available upon request. https://doi.pangaea.de/10.1594/PANGAEA.888518

350 *Author contributions.* This study was initiated and supervised by HM, AB, IW and MS. The field and laboratory data were collected by MS, SH, MG, AB and JK and analysed by SH with support from JK and under supervision of IW and MS. Data processing and calculations were made and interpreted by SH and discussed with JK, IW, and MG. The ice flow was modelled by GJ with input data from MG. The paper was written by SH with comments and suggestions for improvements from all co-authors.

Competing interests. The authors declare that they have no conflict of interest.

References

360 Alley, R. B.: Fabrics in Polar Ice Sheets: Development and Prediction, Science, 240, 493–495, 1988.

Alley, R. B.: Flow-Law Hypotheses for Ice-Sheet Modeling, Journal of Glaciology, 38, 245–256, 1992.

Alley, R. B., Perepezko, J. H., and Bentley, C. R.: Grain Growth in Polar Ice: I. Theory, Journal of Glaciology, 32, 415–424, https://doi.org/10.3189/S0022143000012120, 1986.

Azuma, N.: A Flow Law for Anisotropic Ice and Its Application to Ice Sheets, Earth and Planetary Science Letters, 128, 601–614, 365 https://doi.org/10.1016/0012-821X(94)90173-2, 1994.

Azuma, N. and Higashi, A.: Mechanical Properties of Dye 3 Greenland Deep Ice Cores, Annals of glaciology, 5, 1–8, 1984.

Azuma, N., Miyakoshi, T., Yokoyama, S., and Takata, M.: Impeding Effect of Air Bubbles on Normal Grain Growth of Ice, Journal of Structural Geology, 42, 184–193, https://doi.org/10.1016/j.jsg.2012.05.005, 2012.

Bauder, A., ed.: The Swiss Glaciers 2015/16 and 2016/17, vol. 137/138 of *Glaciological Report*, Cryospheric Commission (EKK) of the 370 Swiss Academy of Sciences (SCNAT), https://doi.org/10.18752/glrep_137-138, 2018.

Binder, T., Garbe, C. S., Wagenbach, D., Freitag, J., and Kipfstuhl, S.: Extraction and Parametrization of Grain Boundary Networks in Glacier Ice, Using a Dedicated Method of Automatic Image Analysis, Journal of Microscopy, 250, 130–141, https://doi.org/10.1111/jmi.12029, 2013.

Budd, W. F.: The Development of Crystal Orientation Fabrics in Moving Ice, Z. Gletscherkd. Glazialgeol, 8, 65–105, 1972.

375 Budd, W. F. and Jacka, T. H.: A Review of Ice Rheology for Ice Sheet Modelling, Cold Regions Science and Technology, 16, 107–144, https://doi.org/10.1016/0165-232X(89)90014-1, 1989.

Budd, W. F., Warner, R. C., Jacka, T. H., Li, J., and Treverrow, A.: Ice Flow Relations for Stress and Strain-Rate Components from Combined Shear and Compression Laboratory Experiments, Journal of Glaciology, 59, 374–392, https://doi.org/10.3189/2013JoG12J106, 2013.

Church, G. J., Bauder, A., Grab, M., Hellmann, S., and Maurer, H.: High-Resolution Helicopter-Borne Ground Penetrating Radar Survey to 380 Determine Glacier Base Topography and the Outlook of a Proglacial Lake, in: 2018 17th International Conference on Ground Penetrating Radar (GPR), pp. 1–4, IEEE, 2018.

Cuffey, K. M. and Paterson, W. S. B.: The Physics of Glaciers, Elsevier, Amsterdam, 4th ed. edn., 2010.

Diez, A. and Eisen, O.: Seismic Wave Propagation in Anisotropic Ice – Part 1: Elasticity Tensor and Derived Quantities from Ice-Core Properties, The Cryosphere, 9, 367–384, https://doi.org/10.5194/tc-9-367-2015, 2015.

385 Duval, P.: Creep and Recrystallization of Polycrystalline Ice, Bulletin de Minéralogie, 102, 80–85, https://doi.org/10.3406/bulmi.1979.7258, 1979.

Duval, P.: Creep and Fabrics of Polycrystalline Ice Under Shear and Compression, Journal of Glaciology, 27, 129–140, https://doi.org/10.3189/S002214300001128X, 1981.

Duval, P. and Castelnau, O.: Dynamic Recrystallization of Ice in Polar Ice Sheets, Le Journal de Physique IV, 5, C3–197, 1995.

390 Eichler, J.: C-Axis Analysis of the NEEM Ice Core–An Approach Based on Digital Image Processing, Diploma Thesis, Freie Universität Berlin, 2013.

Faria, S. H., Freitag, J., and Kipfstuhl, S.: Polar Ice Structure and the Integrity of Ice-Core Paleoclimate Records, Quaternary Science Reviews, 29, 338–351, https://doi.org/10.1016/j.quascirev.2009.10.016, 2010.

Faria, S. H., Weikusat, I., and Azuma, N.: The Microstructure of Polar Ice. Part I: Highlights from Ice Core Research, Journal of Structural 395 Geology, 61, 2–20, https://doi.org/10.1016/j.jsg.2013.09.010, 2014a.

Faria, S. H., Weikusat, I., and Azuma, N.: The Microstructure of Polar Ice. Part II: State of the Art, Journal of Structural Geology, 61, 21–49, https://doi.org/10.1016/j.jsg.2013.11.003, 2014b.

Farinotti, D., Huss, M., Bauder, A., Funk, M., and Truffer, M.: A Method to Estimate the Ice Volume and Ice-Thickness Distribution of Alpine Glaciers, Journal of Glaciology, 55, 422–430, 2009.

400 Gagliardini, O., Zwinger, T., Gillet-Chaulet, F., Durand, G., Favier, L., de Fleurian, B., Greve, R., Malinen, M., Martín, C., Råback, P., Ruokolainen, J., Sacchettini, M., Schäfer, M., Seddik, H., and Thies, J.: Capabilities and Performance of Elmer/Ice, a New-Generation Ice Sheet Model, Geoscientific Model Development, 6, 1299–1318, https://doi.org/10.5194/gmd-6-1299-2013, 2013.

GlaThiDa Consortium: Glacier Thickness Database 3.0.1. World Glacier Monitoring Service, Zurich, Switzerland, https://doi.org/10.5904/wgms-glathida-2019-03, 2019.

405 Gow, A. J. and Meese, D.: Physical Properties, Crystalline Textures and c-Axis Fabrics of the Siple Dome (Antarctica) Ice Core, Journal of Glaciology, 53, 573–584, https://doi.org/10.3189/002214307784409252, 2007.

Gow, A. J. and Williamson, T.: Rheological Implications of the Internal Structure and Crystal Fabrics of the West Antarctic Ice Sheet as Revealed by Deep Core Drilling at Byrd Station, Geological Society of America Bulletin, 87, 1665–1677, 1976.

Grab, M., Bauder, A., Ammann, F., Langhammer, L., Hellmann, S., Church, G. J., Schmid, L., Rabenstein, L., and Maurer, H. R.: Ice Volume
410 Estimates of Swiss Glaciers Using Helicopter-Borne GPR — an Example from the Glacier de La Plaine Morte, in: 2018 17th International Conference on Ground Penetrating Radar (GPR), pp. 1–4, https://doi.org/10.1109/ICGPR.2018.8441613, 2018.

Hambrey, M. J. and Milnes, A. G.: Structural Geology of an Alpine Glacier (Griesgletscher, Valais, Switzerland), Eclogae Geologicae Helvetiae, 70, 667–684, 1977.

Hambrey, M. J., Milnes, A. G., and Siegenthaler, H.: Dynamics and Structure of Griesgletscher, Switzerland, Journal of Glaciology, 25,
415 215–228, https://doi.org/10.3189/S0022143000010455, 1980.

Hellmann, S., Kerch, J., Eichler, J., Jansen, D., Weikusat, I., Schwikowski, M., Bauder, A., and Maurer, H.: Crystal C-Axes Measurements (Fabric Analyser G50) of Ice Core Samples Collected from the Temperate Alpine Ice Core Rhone_2017, https://doi.org/https://doi.org/10.1594/PANGAEA.888518, 2018.

Hooke, R. L.: Structure and Flow in the Margin of the Barnes Ice Cap, Baffin Island, N.W.T., Canada, Journal of Glaciology, 12, 423–438,
420 https://doi.org/10.3189/S0022143000031841, 1973.

Hooke, R. L. and Hudleston, P. J.: Origin of Foliation in Glaciers, Journal of Glaciology, 20, 285–299, https://doi.org/10.3189/S0022143000013848, 1978.

Hooke, R. L. and Hudleston, P. J.: Ice Fabrics in a Vertical Flow Plane, Barnes Ice Cap, Canada, Journal of Glaciology, 25, 195–214, https://doi.org/10.3189/S0022143000010443, 1980.

425 Jacka, T. H. and Jun, L.: The Steady-State Crystal Size of Deforming Ice, Annals of Glaciology, 20, 13–18, https://doi.org/10.3189/1994AoG20-1-13-18, 1994.

Jacka, T. H. and Maccagnan, M.: Ice Crystallographic and Strain Rate Changes with Strain in Compression and Extension, Cold Regions Science and Technology, 8, 269–286, https://doi.org/10.1016/0165-232X(84)90058-2, 1984.

Jansen, D., Llorens Verde, M. G., Westhoff, J., Steinbach, F., Kipfstuhl, S., Bons, P. D., Griera, A., and Weikusat, I.: Small-Scale Dis-
430 turbances in the Stratigraphy of the NEEM Ice Core: Observations and Numerical Model Simulations, The Cryosphere, 10, 359–370, https://doi.org/Jansen, D. , Llorens Verde, M. G. , Westhoff, J. , Steinbach, F. , Kipfstuhl, S. , Bons, P. D. , Griera, A. and Weikusat, I. ORCID: https://orcid.org/0000-0002-3023-6036 <https://orcid.org/0000-0002-3023-6036> (2016) Small-scale disturbances

in the stratigraphy of the NEEM ice core: observations and numerical model simulations , The Cryosphere, 10 , pp. 359-370 . doi:https://doi.org/10.5194/tc-10-359-2016 <https://doi.org/10.5194/tc-10-359-2016> , hdl:10013/epic.46883, 2016.

435 Journaux, B., Chauve, T., Montagnat, M., Tommasi, A., Barou, F., Mainprice, D., and Gest, L.: Recrystallization Processes, Microstructure and Crystallographic Preferred Orientation Evolution in Polycrystalline Ice during High-Temperature Simple Shear, The Cryosphere, 13, 1495–1511, https://doi.org/https://doi.org/10.5194/tc-13-1495-2019, 2019.

Jouvet, G., Huss, M., Funk, M., and Blatter, H.: Modelling the Retreat of Grosser Aletschgletscher, Switzerland, in a Changing Climate, Journal of Glaciology, 57, 1033–1045, https://doi.org/10.3189/002214311798843359, 2011.

440 Kamb, B.: Experimental Recrystallization of Ice under Stress, Washington DC American Geophysical Union Geophysical Monograph Series, 16, 211, https://doi.org/10.1029/GM016p0211, 1972.

Kamb, W. B.: Ice Petrofabric Observations from Blue Glacier, Washington, in Relation to Theory and Experiment, Journal of Geophysical Research, 64, 1891–1909, https://doi.org/10.1029/JZ064i011p01891, 1959.

Krischke, A., Oechsner, U., and Kipfstuhl, S.: Rapid Microstructure Analysis of Polar Ice Cores, Optik & Photonik, 10, 32–35,
445 https://doi.org/10.1002/opph.201500016, _eprint: https://onlinelibrary.wiley.com/doi/pdf/10.1002/opph.201500016, 2015.

Kuiper, E.-J. N., de Bresser, J. H. P., Drury, M. R., Eichler, J., Pennock, G. M., and Weikusat, I.: Using a Composite Flow Law to Model Deformation in the NEEM Deep Ice Core, Greenland: Part 2 the Role of Grain Size and Premelting on Ice Deformation at High Homologous Temperature, The Cryosphere Discussions, pp. 1–30, https://doi.org/https://doi.org/10.5194/tc-2018-275, 2019.

Lipenkov, V. Y., Barkov, N. I., Duval, P., and Pimienta, P.: Crystalline Texture of the 2083 m Ice Core at Vostok Station, Antarctica, Journal
450 of Glaciology, 35, 392–398, https://doi.org/10.3189/S0022143000009321, 1989.

Llorens, M.-G., Griera, A., Bons, P. D., Lebensohn, R. A., Evans, L. A., Jansen, D., and Weikusat, I.: Full-Field Predictions of Ice Dynamic Recrystallisation under Simple Shear Conditions, Earth and Planetary Science Letters, 450, 233–242, https://doi.org/10.1016/j.epsl.2016.06.045, 2016.

Maohuan, H., Ohtomo, M., and Wakahama, G.: Transition in Preferred Orientation of Polycrystalline Ice from Repeated Recrystallization,
455 Annals of Glaciology, 6, 263–264, https://doi.org/10.3189/1985AoG6-1-263-264, 1985.

Matsuda, M. and Wakahama, G.: Crystallographic Structure of Polycrystalline Ice, Journal of Glaciology, 21, 607–620, https://doi.org/10.3189/S0022143000033724, 1978.

Montagnat, M., Azuma, N., Dahl-Jensen, D., Eichler, J., Fujita, S., Gillet-Chaulet, F., Kipfstuhl, S., Samyn, D., Svensson, A., and Weikusat, I.: Fabric along the NEEM Ice Core, Greenland, and Its Comparison with GRIP and NGRIP Ice Cores, The Cryosphere, 8, 1129–1138,
460 https://doi.org/10.5194/tc-8-1129-2014, 2014.

Patrick, B. A., Corvino, A. F., and Wilson, C. J. L.: Ice-Flow Measurements and Deformation at Marginal Shear Zones on Sørsdal Glacier, Ingrid Christensen Coast, East Antarctica, Annals of Glaciology, 37, 60–68, https://doi.org/10.3189/172756403781815933, 2003.

Peternell, M., Kohlmann, F., Wilson, C. J., Seiler, C., and Gleadow, A. J.: A New Approach to Crystallographic Orientation Measurement for Apatite Fission Track Analysis: Effects of Crystal Morphology and Implications for Automation, Chemical Geology, 265, 527–539,
465 https://doi.org/10.1016/j.chemgeo.2009.05.021, 2009.

Petit, J. R., Jouzel, J., Raynaud, D., Barkov, N. I., Barnola, J.-M., Basile, I., Bender, M., Chappellaz, J., Davis, M., Delaygue, G., Delmotte, M., Kotlyakov, V. M., Legrand, M., Lipenkov, V. Y., Lorius, C., PÉpin, L., Ritz, C., Saltzman, E., and Stievenard, M.: Climate and Atmospheric History of the Past 420,000 Years from the Vostok Ice Core, Antarctica, Nature, 399, 429–436, https://doi.org/10.1038/20859, 1999.

The Cryosphere
Discussions

EGU
Open Access

470   Qi, C., Prior, D. J., Craw, L., Fan, S., Llorens, M.-G., Griera, A., Negrini, M., Bons, P. D., and Goldsby, D. L.: Crystallographic Preferred
Orientations of Ice Deformed in Direct-Shear Experiments at Low Temperatures, The Cryosphere, 13, 351–371, 2019.

Rigsby, G. P.: Crystal Fabric Studies on Emmons Glacier Mount Rainier, Washington, The Journal of Geology, 59, 590–598, 1951.

Rigsby, G. P.: Crystal Orientation in Glacier and in Experimentally Deformed Ice, Journal of Glaciology, 3, 589–606, 1960.

Robin, G. D. Q., Mitchell, G. F., and West, R. G.: Ice Cores and Climatic Change, Philosophical Transactions of the Royal Society of London.
475   B, Biological Sciences, 280, 143–168, https://doi.org/10.1098/rstb.1977.0103, 1977.

Russell-Head, D. S. and Budd, W. F.: Ice-Sheet Flow Properties Derived from Bore-Hole Shear Measurements Combined With Ice-Core
Studies, Journal of Glaciology, 24, 117–130, https://doi.org/10.3189/S0022143000014684, 1979.

Schulson, E. M. and Duval, P.: Creep and Fracture of Ice, 2009.

Schwikowski, M., Jenk, T. M., Stampfli, D., and Stampfli, F.: A New Thermal Drilling System for High-Altitude or Temperate Glaciers,
480   Annals of Glaciology, 55, 131–136, https://doi.org/10.3189/2014AoG68A024, 2014.

Thompson, L. G., Mosley-Thompson, E., Davis, M. E., Henderson, K. A., Brecher, H. H., Zagorodnov, V. S., Mashiotta, T. A., Lin, P.-N.,
Mikhalenko, V. N., Hardy, D. R., and Beer, J.: Kilimanjaro Ice Core Records: Evidence of Holocene Climate Change in Tropical Africa,
Science, 298, 589–593, https://doi.org/10.1126/science.1073198, 2002.

Thorsteinsson, T., Kipfstuhl, J., and Miller, H.: Textures and Fabrics in the GRIP Ice Core, Journal of Geophysical Research: Oceans, 102,
485   26 583–26 599, https://doi.org/10.1029/97JC00161, 1997.

Thwaites, R. J., Wilson, C. J. L., and McCray, A. P.: Relationship Between Bore-Hole Closure and Crystal Fabrics in Antarctic Ice Core from
Cape Folger, Journal of Glaciology, 30, 171–179, https://doi.org/10.3189/S0022143000005906, 1984.

Tison, J.-L. and Hubbard, B.: Ice Crystallographic Evolution at a Temperate Glacier: Glacier de Tsanfleuron, Switzerland, Geological Society,
London, Special Publications, 176, 23–38, 2000.

490   Vollmer, F. W.: C Program for Automatic Contouring of Spherical Orientation Data Using a Modified Kamb Method, Computers & Geo-
sciences, 21, 31–49, 1995.

Wallbrecher, E.: Tektonische Und Gefügeanalytische Arbeitsweisen: Graphische, Rechnerische Und Statistische Verfahren, Enke, Stuttgart,
1986.

Weikusat, I., Kipfstuhl, S., Azuma, N., Faria, S. H., and Miyamoto, A.: Deformation Microstructures in an Antarctic Ice Core (EDML) and
495   in Experimentally Deformed Artificial Ice, Low Temperature Science, 68, 115–123, 2009a.

Weikusat, I., Kipfstuhl, S., Faria, S. H., Azuma, N., and Miyamoto, A.: Subgrain Boundaries and Related Microstructural Features in EDML
(Antarctica) Deep Ice Core, Journal of Glaciology, 55, 461–472, https://doi.org/10.3189/002214309788816614, 2009b.

Weikusat, I., Jansen, D., Binder, T., Eichler, J., Faria, S. H., Wilhelms, F., Kipfstuhl, S., Sheldon, S., Miller, H., Dahl-Jensen, D., and Kleiner,
T.: Physical Analysis of an Antarctic Ice Core—towards an Integration of Micro- and Macrodynamics of Polar Ice, Philosophical Transac-
500   tions of the Royal Society A: Mathematical, Physical and Engineering Sciences, 375, 20150 347, https://doi.org/10.1098/rsta.2015.0347,
2017.

Wilson, C. J., Russell-Head, D. S., and Sim, H. M.: The Application of an Automated Fabric Analyzer System to the Textural Evolution of
Folded Ice Layers in Shear Zones, Annals of Glaciology, 37, 7–17, 2003.

Wilson, C. J. L. and Peternell, M.: Evaluating Ice Fabrics Using Fabric Analyser Techniques in Sørsdal Glacier, East Antarctica, Journal of
505   Glaciology, 57, 881–894, https://doi.org/10.3189/002214311798043744, 2011.